Circumstellar Disk Modeling with Bayesian Statistics and Marginal Probabilities

Swarthmore College Thesis by Andrew Skemer
Advisor: Eric L.N. Jensen

Abstract:

This paper summarizes current knowledge of circumstellar debris disks and presents methods of modeling optically thin disks. The techniques of Bayesian statistics and marginal probabilities are applied to the disk modeling problem so that I can construct probability distributions for individual disk parameters. I apply these methods and interpret the results for three stars: HD 105, HD 107146, and HD 115043.

In the introduction, I give background information on circumstellar disks, and their possible connection with dust in the Solar System. I describe the general technique of modeling infrared excesses, and present the goals of this paper. Because the stars I study are unresolved in the wavelength range of dust emission, the flux contributions of a star and its disk must be separated before I can model the disk parameters. To do that, I model the star's photosphere, and subtract its contribution from the data.

In the body of the paper, I describe the data and the modeling procedures for the photosphere and the circumstellar disk. I present the methods of Bayesian statistics and marginal probabilities as they apply to this paper, and I use the techniques to analyze the three star sample. The methods of Bayesian/marginal statistics reveal probability distributions of seven disk modeling parameters for each star, and in many cases, place constraints on important parameters such as inner radius and disk mass. HD 107146 has a resolved disk in scattered light, and the results of my marginal distributions are compared to the resolved data. I also examine the results of HD 107146 with and without millimeter data to demonstrate the usefulness of long-wavelength observations for constraining the disk's inner radius and dust absorption/emission parameters. I conclude the paper with a list of future steps—both short-term and long-term.

1. Introduction

Circumstellar disks are disks of dust and gas around young stars, remnant of the star formation process. Studying them provides insight into the evolution of our own Solar System, and provides the key connection between star and planet formation. It used to be impossible to detect disks except around hot, nearby stars with extremely young, optically thick disks. With the launch of the Spitzer Space Telescope, we enjoy a powerful new tool for studying a much wider range of circumstellar disks, including ones that surround Solar-type stars and could possibly contain Earth-like planets.

This introduction is meant to summarize necessary background on circumstellar disks and present a road-map for the rest of the paper.

I present the background information in two parts. In the circumstellar disk section, I give a brief history of circumstellar disk discovery, give examples of large resolved disks, and explain how the disks I study are different from those. I briefly discuss the formation of circumstellar disks, and explain how dust removal mechanisms indicate the presence of large, dynamically stable grains, which fragment to replenish the small grain supply that dominates disk emission. In the Solar System section, I present three categories of dust (Zodiacal Dust, Kuiper Belt dust, and Oort Cloud dust), and discuss their merits as candidate constituents of circumstellar disks with respect to their visibility from outside the Solar System. I then describe the direction of the rest of the paper. Specifically, I discuss the different types of results I seek, and the purpose of each of my primary techniques.

1.1. Circumstellar Disks

As part of the star-forming process, giant molecular clouds fragment and collapse into young stars surrounded by disks of dust and gas. These circumstellar disks can be the location of planet formation, and their evolution is closely tied with our Solar System's.

The first circumstellar disks were discovered by IRAS (Infrared Astronomy Satellite) scientists who were measuring zero-point fluxes by observing Vega and other A stars (Aumann *et al.* 1984). In each case, by showing that there was more infrared flux than could be accounted for by the star alone, the IRAS team showed that something else was emitting light; they posited disks of dust that were heated by the star. Within a year, Smith and Terrile (1984) published resolved images of the Beta Pictoris circumstellar system confirming that it is a 1000 AU radius, edge-on disk (Fig. 1).

Young stars are the primary locations for circumstellar disks. As a protostar collapses during star formation, residual dust from the molecular cloud is pulled in gravitationally, while angular momentum causes it to flatten into a Keplerian, orbiting disk. By the time the disk becomes optically thin through accretion and dust consolidation, radiative processes are constantly removing dust from the system (Backman and Paresce 1993). Poynting-Robertson drag pulls fast-orbiting small dust particles into an inward spiral, while radiation pressure blows other small dust out of the system. Ice sublimation turns ice into gas close to the star. Collisions can fragment larger dust grains so that radiative processes can remove them. Adding the effects of these mechanisms reveals that with a static supply of small grains, an optically thin circumstellar disk would disappear quickly, sometimes well within a million years (Backman and Paresce 1993). However, many stars older than a million years have been observed to have circumstellar disks. This is most likely because large objects are colliding, and fragmenting to replenish the dust supply (Backman and Paresce 1993).

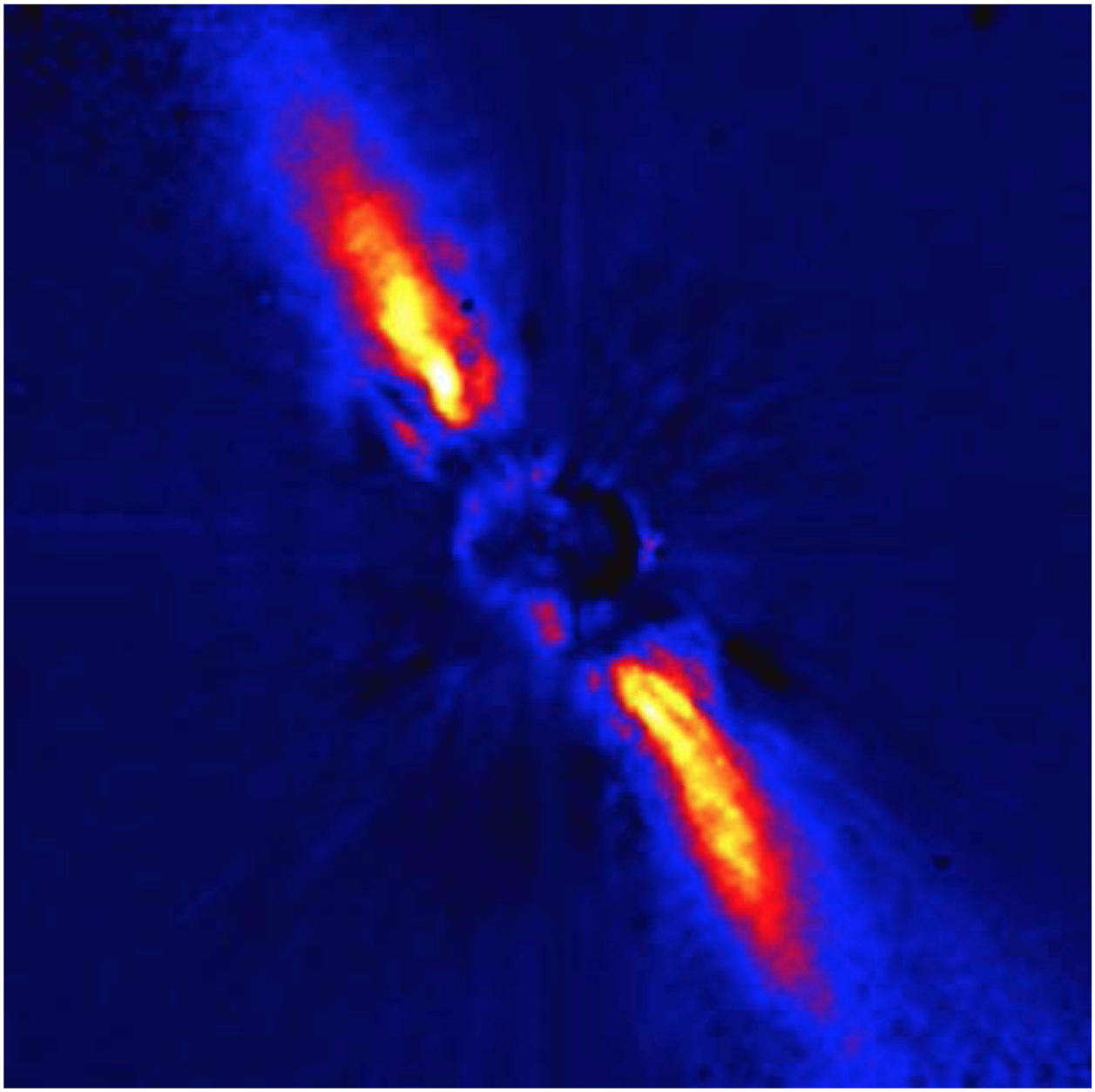

Fig. 1.— Resolved images of Beta Pictoris, Fomalhaut and Vega proved the existence of circumstellar disks. In this image of Beta Pictoris, taken by the European Southern Observatory (J. Beuzit 1997), a coronagraph has blocked the contaminating light of the star, leaving a 1.25 μm, false-color image of an almost edge on disk. The radius of Beta Pictoris' disk is about 1000 AU, and the dust is optically thick (unlike the disks studied in this paper). The perturbation in the bottom right limb could be the result of an orbiting planet, or a harmonic effect from a close-passing star (Kalas *et al.* 2000).

1.2. Dust in the Solar System

It is only by understanding the physics of our own Solar System that we will be able to understand other circumstellar systems and vice-versa. Much of the interest in circumstellar disks concerns the comparison of dust parameters with observation and direct measurements in the Solar System. The Solar System has three major groups of dust: Zodiacal dust, Kuiper Belt dust, and Oort Cloud dust. Together, these masses compose the Sun's circumstellar disk, although each individual component would not necessarily be observable from an external system.

The Zodiacal Dust is interplanetary dust commonly associated with the asteroid belt. Located at 3 AU, it only has 10^{-10} the mass of the planets (Backman and Paresce 1993). At 20 μm, it emits 0.1% of the light that the Sun emits (Backman and Paresce 1993), and could not be detected by our most sophisticated instruments from outside the Solar System.

The Oort Cloud is a 100 $M_{\oplus}$ collection of comets, spherically distributed, that orbit between 0.1 and 0.75 parsecs from Earth (Backman and Paresce 1993). At that distance, the dust is only about 5 K (Backman and Paresce 1993), so that even if it has a lot of surface area, it will blend in with the ISM background. Stars are on average about 1 pc away from each other in the Solar neighborhood, so the clouds of comets probably overlap and exchange mass in most cases, which would contribute to the ISM blending effect. The circumstellar disks that have been observed have dust that is too hot to be part of a long-orbit comet cloud, and it is unlikely that the Oort Cloud could be detected from another star.

The Kuiper Belt is the Solar System's best candidate to be a detectable circumstellar disk from interstellar distances. It exists between 30 and 115 AU (Jewitt and Luu 2000) (a reasonable pair of parameters based on measurements of circumstellar disk radii), and it has a mixed size distribution of grains, with enough small particles to make its surface area and emission observable (Backman and Paresce 1993). The Kuiper Belt has less mass (perhaps by a factor of 100) in its inner region (30-42 AU) than its outer region (>50 AU) because of Neptune's gravitational perturbation (Jewitt and Luu 2000). If extra-solar circumstellar systems have massive planets, dust might be depleted in their inner disk regions.

If the Kuiper Belt is truly the Sun's detectable circumstellar disk, we are lucky to enjoy a few different ways of studying it. Most Kuiper Belt studies have concentrated on the detection of large objects. Indeed, Pluto is thought to be a Kuiper Belt object along with the more recently discovered Sedna. Mass limits on the Kuiper Belt have been placed by COBE (Cosmic Background Explorer) and Voyager, which actually measured impacts with small Kuiper Belt Objects. The limits, $< 10^{-5}$ Earth Masses and $> 10^{-8}$ Earth masses respectively, are contingent on the chosen grain distribution model—Voyager was only capable of detecting grains more massive than $1.2 \cdot 10^{-8}$ kg (Jewitt and Luu 2000), which would be $80\,\mu m$ radius spheres using $\rho = 5 g/cm^3$. Other physical properties of the grains, specifically their radiative properties, are of interest to those who study circumstellar disks.

1.3. Goals and Methods

The purpose of this paper is to examine the properties of circumstellar disks observed with the Spitzer Infrared Space Telescope, and demonstrate the power of the Bayesian/marginal technique. Our primary mechanism is to construct model disks, based on theory and observation of dust within our own Solar System. Model disks' emission is compared to the observed stars' infrared emission by subtracting out the contribution of the stellar photosphere, leaving an infrared excess (Fig. 2). The theory and results are presented in several ways:

1. First, I calculate a best-fit (least-squares) model disk. Because Spitzer photometry can only provide a few data points, and the disk models have many more free parameters, I estimate the values of several parameters based on outside information. While the goodness-of-fit of this model can be calculated with a reduced $\chi 2$, the relative likelihood of the model is still unknown; there could be several more models that fit almost as well. The purpose of the best-fit model in this context is not to determine the correct model, but to determine whether a model can fit the data at all.

2. The quantities that we really want to calculate are the probability distributions of the important disk parameter (mass, inner/outer radius, etc.). I use Bayesian statistics to assign relative probabilities based on the models' $\chi 2$ values, and use the method of marginal probabilities to integrate over a large grid of possible models. This allows me to directly calculate probability distributions and assign confidence intervals to individual disk parameters.

3. I explore the sensitivity of long-wavelength (mm) data to relevant disk parameters. By calculating the marginal probabilities of disk parameters for HD 107146 with and without the long-wavelength data, I demonstrate the worth of a particular set of ancillary data.

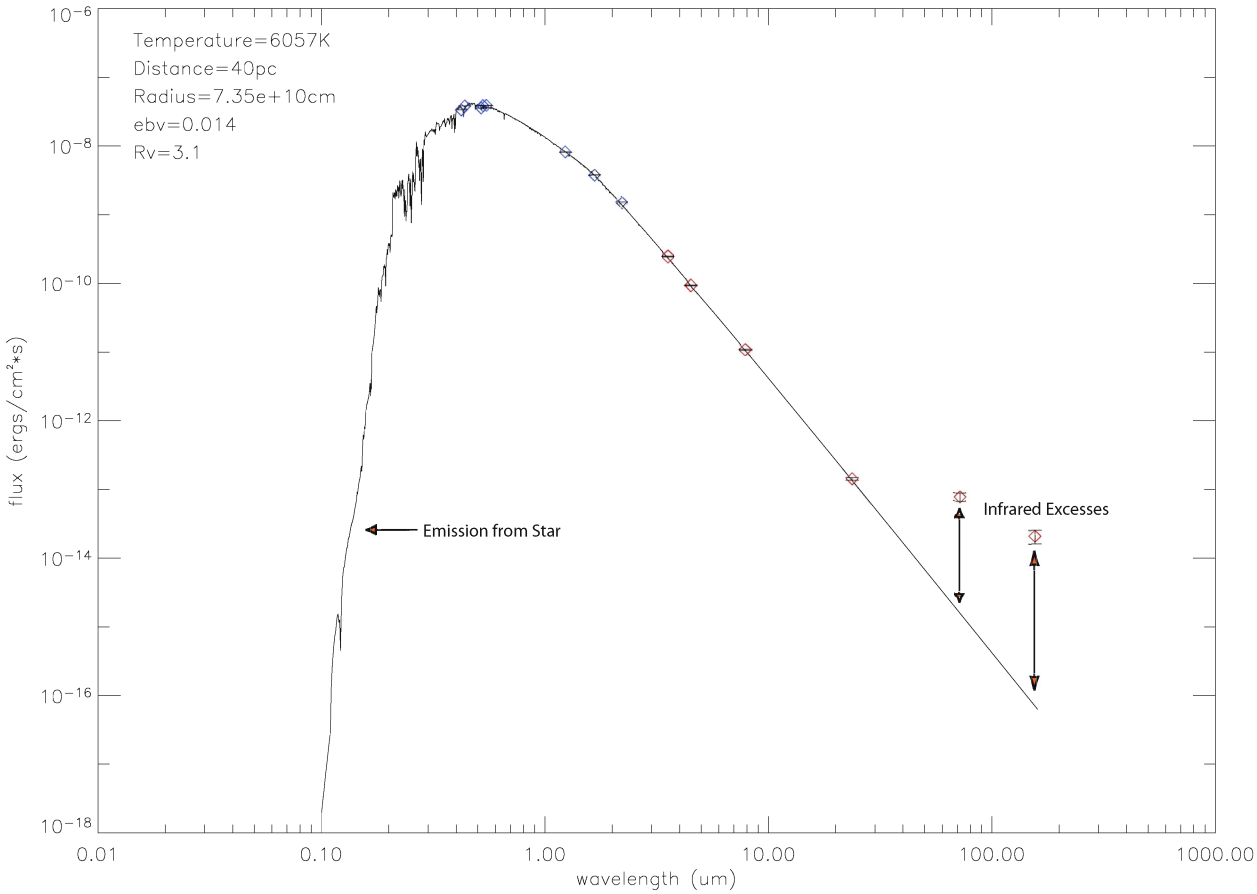

Fig. 2.— The blue diamonds are optical and near-IR data fit with a model atmosphere. Even though the model is consistent with the four infrared points between 3.6 and 24 microns, I do not use them in the photosphere fit to avoid contamination from the circumstellar disk. The 70 and 160 microns points are well above the expected stellar emission, which indicates the presence of a circumstellar disk. The magnitudes of the excesses are used to model the disk's physical properties.

2. Photosphere Fit

The first step in calculating the parameters of a circumstellar disk model is to determine the contribution of a stellar photosphere to the observed infrared photometry. To do this, I fit a model atmosphere to data that has not been contaminated by the flux of a circumstellar disk. Since the disks are much cooler than the stars they surround, they contribute a negligible flux in the optical bands. For the stars in this paper, circumstellar disks do not emit substantial flux at wavelengths shorter than the Spitzer wavelengths ($< 3.6\ \mu m$). This can be confirmed for each star after the photosphere fit.

2.1. Photometry Data

The stars in this paper all have Tycho-2/Hipparcos and 2MASS photometric data, which amounts to six data points: Hp, Bt, Vt in the optical and J, H, and Ks in the near-infrared. Sometimes ground-based optical photometry is available from other papers; I primarily use Johnson-Cousins photometry, but I am capable of using any filters that have a calibrated filter profile. Data points in complete disagreement with the majority are not used. Hipparcos parallax measurements are necessary for determining the distance to the star, which is used in the photosphere modeling program to calculate the stellar radius.

2.2. The Least-Squares Fit and Free Parameters

The photosphere fitting program converts photometric data to energy fluxes using zero-point in-band fluxes calculated by convolving filter profiles with a model atmosphere of Vega (by Robert Kurucz through private communication with John Carpenter). The zero-point in-band fluxes match the literature's to within one percent in most cases (Cohen *et al.* 2003a,b; Bessell 2000). I run a Levenberg-Marquardt algorithm, least-squares fitting program with temperature, stellar radius (as the normalization parameter), and extinction (for stars farther than the 40 pc "Local Bubble" (Meyer *et al.* 2004)) as free parameters.

The program uses Kurucz (1993) model atmospheres with solar metallicity and linearly interpolates the temperature between the two nearest models, which have a 250K spacing. The models are reddened using a parameterization by Fitzpatrick (1999). Finally, the program calculates the model in-band fluxes by convolving the Kurucz model with filter/atmosphere/detector transmission curves. The photosphere model fitting program returns the star's temperature, radius, and extinction.

I calculate the reduced $\chi 2$ as a basic goodness-of-fit parameter, but the error analysis can easily become much more complicated. Though I do not explicitly calculate error bars for the individual disk parameters, I expect them to be small. The fit of the near-infrared photometry is most

important in establishing the Rayleigh-Jeans blackbody tail for calculating excesses. The optical photometry is most important for distinguishing the contributions of temperature and radius, which is important when using luminosity as a parameter in the disk modeling program.

	HD 105	HD 107146	HD 115043
D (pc)	40	28	25
R ($R_\odot$)	1.06	1.00	0.99
T (K)	6057	5862	5845
R_V	3.1	3.1	3.1
E(B-V)	0.014	0.000	0.000
χ^2_ν	1.26	2.68	1.27

Table 1: Best-fit model atmosphere results for the three stars in this paper. D, R, and T are fit for all three models. Rv is always fixed. E(B-V) is only fit for HD 105, which is at the outer edge of the 40 pc "Local Bubble" (Meyer *et al.* 2004). The model atmospheres are Kurucz (1993) models with solar metallicity.

3. Disk Modeling

3.1. Photometry Data

The infrared photometry used to calculate disk parameters is public data supplied by the FEPS (Formation and Evolution of Planetary Systems) Spitzer Legacy Project (Meyer *et al.* 2004). Led by principal investigator Michael Meyer, the FEPS team studies the evolution of circumstellar disks by observing disks in different age groups, all of which belong to stars similar to the Sun. Spitzer Legacy Projects release a public data package with calibrated photometry measurements early in their respective data analysis processes. The FEPS team has released data from three Spitzer instruments: IRAC (near-infrared photometry), IRS (near-infrared spectroscopic data) and MIPS (far-infrared photometry). The IRS data is mostly used to look for spectral lines from the circumstellar disks, which can give information about dust composition. The FEPS team has also integrated sections of the IRS data to construct photometry points. In this paper, I concentrate on the IRAC and MIPS photometry.

Spitzer photometry alone cannot constrain certain disk parameters. I make use of ground-based support observations including mid-IR (Keck) and sub-millimeter (SCUBA-Submillimeter Common User Bolometric Array) data for HD 107146 (Williams *et al.* 2004) and millimeter (SEST-Swedish ESO Submillimetre Telescope) data for most FEPS stars (Carpenter *et al.* 2005)-(though in this paper, SEST data is only used for HD 107146).

The IRAC data are useful for limiting the inner radius of the circumstellar disk, but rarely shows an excess. Some MIPS 24 μm data show disk excesses, and some do not. MIPS 70 μm and 160 μm data almost always have excesses for stars with circumstellar disks. Because of the Earth's atmosphere, and the extremely cold temperatures under which far-infrared data must be taken, Spitzer's most important scientific contributions come from the MIPS instrument. So far, it has been difficult to obtain accurate data with the MIPS 160 μm filter due to a problem with the instrument. The FEPS team has not released nearly as much data at this wavelength as at others.

3.2. Equations and Assumptions

All of the disks studied in this paper are assumed to be optically thin. This can be verified for specific models by checking that σ_0 (the maximum covering fraction/surface density as defined below) is < 1. The condition is necessary so that dust sees the star's light, and Spitzer can see the dust's light. The dust grains are assumed to be in thermal equilibrium, and absorb and emit light without spectral features. The circumstellar disks are azimuthally symmetric, and dust orbits are Keplerian. Accretion from Poynting-Robertson drag and other dynamical forces should produce negligible additions to flux data. If small dust grains are being removed from the system, large, undetected dust should be colliding and fragmenting to replenish the supply. By this mechanism, the disk's mass should decline over time, but small grain emission will be detectable for a period of

time that is long enough to explain the disks we see.

The disk modeling program starts by subtracting model photospheric fluxes (derived as explained in section 2.2) from the data to find infrared excesses. FEPS data is converted to energy flux ($ergs/cm^2 \cdot s$) using wavelengths supplied in the FEPS Data Explanatory Supplement (Hines 2005). A two percent error is added to photometric flux errors in quadrature with the original errors to account for a two percent uncertainty in the Kurucz (1993) model atmospheres (Cohen *et al.* 2003a). The disk model uses equations for an optically thin circumstellar disk following the general outline of (Backman and Paresce 1993) (see Appendix A for details and a complete derivation). The equations model dust temperature as a function of radius, and energy flux as a function of frequency:

$$T_{dust} = [\frac{T_{star}^p L_{star}}{16\pi r^2 \sigma_{SB}} \cdot (\frac{\lambda_0 k}{hc})^{p-q} \cdot \frac{\Gamma(4+p)}{\Gamma(4+q)} \cdot \frac{\Sigma_{i=1}^{\infty} i^{-(4+p)}}{\Sigma_{i=1}^{\infty} i^{-(4+q)}}]^{\frac{1}{4+q}} \tag{1}$$

$$F_\nu = \int_{r_1}^{r_2} \sigma_0 (\frac{r}{r_0})^\gamma (\frac{\xi a \nu}{c})^q B_\nu [T_{dust}(r,a)] \frac{2\pi r dr}{D^2} \tag{2}$$

Within these equations is the implicit assumption that the disk has a power law density drop-off (see definitions of γ and σ_0 below), which allows the calculation of disk mass:

$$M = \frac{8\pi a \rho \sigma_0 (r_2^{\gamma+2} - r_1^{\gamma+2})}{3 r_0^\gamma (\gamma+2)} \tag{3}$$

The quantities in these formulas are defined as follows:

r_0	normalization radius corresponding with density σ_0
r_1	inner disk radius
r_2	outer disk radius
a	grain radius
ρ	grain density
p	power law decay exponent for grain absorption with wavelength— $\epsilon_\lambda = \epsilon_0 (\frac{\lambda}{\lambda_0})^{-p}$
q	power law decay exponent for grain emission with wavelength— $\epsilon_\lambda = \epsilon_0 (\frac{\lambda}{\lambda_0})^{-q}$
λ_0	critical wavelength for which grains absorb/emit like blackbodies at shorter wavelengths, and with a power law decay at longer wavelengths
ξ	$\xi \equiv \lambda_0 / a$—For this paper, $\xi = 1$ (see section 3.4).

γ power law decay of disk surface density with radius— $\sigma = \sigma_0(r/r_0)^\gamma$ where γ is negative

σ_0 geometric surface density of the disk at radius r_0 in units of area/area, i.e. fractional covering of the disk surface by dust.

3.3. An Unphysical Absorption/Emission Approximation used in the Disk Model Equations

Though the details of the disk model equation derivations are left to Appendix A, it is appropriate to point out that the models I use allow power-law growth of emission/absorption for wavelengths short of the critical wavelength, so that $\epsilon > 1$ (Fig. 3). The physical model that I wish to emulate (for $\lambda > \lambda_0$, $\epsilon_\lambda = (\lambda_0/\lambda)^p$ and for $\lambda < \lambda_0$, $\epsilon_\lambda = 1$), gives a non-analytic form for (equations 1 and 2). So I use an unphysical model ($\epsilon_\lambda = (\lambda_0/\lambda)^p$ for all λ) that serves as a good approximation for grain sizes short of the infrared excess wavelengths, and provides an analytic solution to the disk modeling equations.

If the grain size is smaller than the star's peak wavelength, then the grains will absorb and emit at wavelengths longer than the critical wavelength, λ_0, and are accurately modeled. If the grain size is between the peak wavelength of the star and the peak wavelength of the disk, then emission will be modeled properly, and absorption will be modeled somewhat inaccurately. If $p = 0$, then the power-law decay problem is irrelevant, and this is a situation that applies to some of the models described below. Models with grains larger than the peak wavelength of the disk will be modeled inaccurately for both emission and absorption unless $p = q = 0$ (i.e. perfect blackbody grains).

Using the correct equations is an ultimate goal for this project, but it will demand a large increase in computer time. For the time being, large grain radius disk models are physically inaccurate, and this is why multiple-grain-size models cannot be used.

3.4. Limits on Parameters

The purpose of this section is to put limits on the model parameters listed in section 3.2 based on the astronomical literature. The limits come from a wide variety of sources, including laboratory physics, theory, direct spacecraft measurements, and observation. I should stress that many of the limits are very roughly known. When I actually test the fits of the models, I sometimes have to adjust the limits based on my own results.

r_1 Since the stars in this paper are all Solar type stars, the best way to estimate r_1 (until we better understand the dynamics of circumstellar disks or can resolve their inner regions)

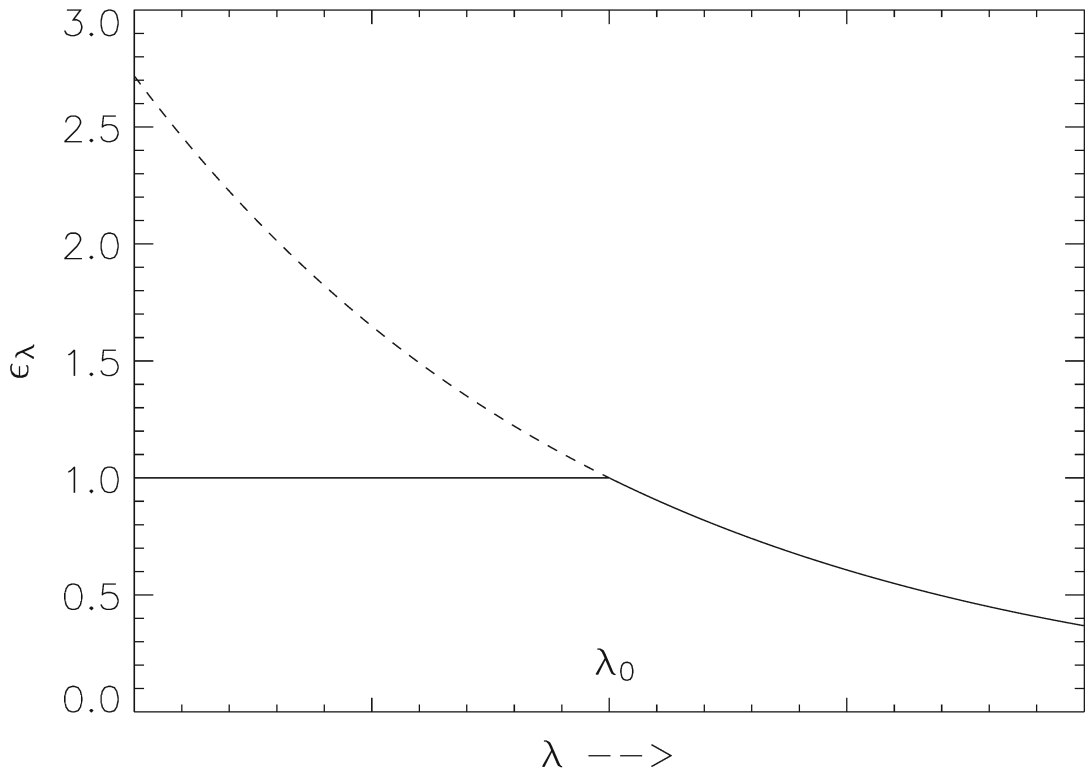

Fig. 3.— The solid line is the correct model for grain emission. Because its use precludes an analytic set of disk modeling equations, I use the dashed line model, which is physically inaccurate, but provides a good estimation for small-grain models.

is to look at the inner radius of the Sun's Kuiper Belt. According to Jewitt and Luu (2000), the range of semi-major axes of known Kuiper Belt objects is 35-115 AU with a depleted region from 30-42 AU. Physically, the inner radius might be set by radiative forces or sweeping planetesimals (Neptune in the case of our Solar System), which means inner radius might correlate with disk mass and/or age. This makes the Solar estimate not applicable to all the circumstellar disks in the FEPS sample, so the models in this paper use very loose constraints for r_1.

r_2 The outer radii of the circumstellar disks are also loosely constrained, but because Spitzer photometry is best suited for studying the hot inner regions of disks, the data in this paper are not sensitive to outer radius anyway. To constrain the outer radius, I tentatively use a lower bound of 115 AU, the largest semi-major axes of known Kuiper Belt objects (Jewitt and Luu 2000), and 1000 AU, the resolved outer radius of Beta Pictoris (Jewitt and Luu 2000), as the range of r_2 values. Because some papers have suggested ring-like circumstellar disks (Hines *et al.* 2006; Ardila *et al.* 2004), the de facto constraint I use for a lower limit is that $r_2 > r_1$. Any dust extending much farther than 1000 AU would be undetected against background by the instruments used in this paper.

a Grains in circumstellar disks have a wide distribution of radii, from μm to planetesimal. The models in this paper are single grain-size models; the grain size, a, most closely corresponds to the smallest grain size in the true distribution, because these grains emit the majority of the disk's light. Radiation pressure and Poynting-Robertson drag remove small dust grains from the system. Though it is commonly posited that small grains are replenished by larger particles that collide and fragment, the very short time scales allowed by dust removing processes put a lower bound on a. Hines *et al.* (2006) use a blow-out size (the lower limit on radius for grains stable to radiative forces) of 0.5 μm. A grain of this size will be forced out of the system by radiation pressure in 8 years if it starts at 6 AU or 80 years if it starts at 30 AU (Hines *et al.* 2006). However, this analysis assumes perfect blackbody grains, and ignores the fact that extremely small grains are inefficient absorbers/emitters at stellar wavelengths, which would dampen the magnitude of the effect (Soter *et al.* 1977; Burns *et al.* 1979). Hines *et al.* (2006) assume that grains in the range between 0.05 and 0.5 μm will be ejected from the system. Grains smaller than 0.05 μm are not significantly affected by radiation forces, but are affected by the solar wind and interplanetary magnetic fields (Soter *et al.* 1977). The dynamics of grains smaller than 0.5 μm are outside the scope of the models discussed in this paper, so I use 0.5 μm as the lower limit on grain size.

The disk modeling equations used in this paper assume a power law decay of absorbing/emitting efficiency with wavelength, but in order to make the disk equations analytic, I allow efficiency to rise above 1 at wavelengths short of the critical wavelength (see section 3.3). For this reason, large grains (which have large critical wavelengths),

are modeled nonphysically. Since the stars in this paper have negligible excesses at wavelengths shorter than 24 μm, I use 24 μm as a rough upper limit for grain size. This is also the reason I do not use a multiple grain size model, which would require larger grain sizes than my models can accurately represent.

ρ — The density of the grains is only important for determining the mass of the disk. The density of Earth is 5.52 g/cm^3 (Carroll and Ostlie 1996). Hines *et al.* (2006) use 2.5 g/cm^3 as the density of a typical astronomical silicate. I use 5 g/cm^3. The disk mass results can easily be adjusted for a different density.

p and q — Backman and Paresce (1993) list examples of reasonable p and q values. For blackbody grains, $p = q = 0$. For grains larger than the star's peak wavelength, but smaller than the disk's peak wavelength, $p = 0$, $q > 0$. For very small, ISM grains, $p = q = 1.5$. The models presented in this paper allow p and q to vary from 0 to 1.5 with the condition that $p < q$ (the other permutations may be physically implausible based on the examples from Backman and Paresce (1993)).

γ — Beta Pictoris' power law surface density decay constant is -1.7 (Backman and Paresce 1993). The models presented in this paper allow γ to vary from -1.8 to -1.4. γ and r_2 are tightly correlated for the models in this paper, so that a large decay constant corresponds to a large outer radius. Even with mm data to sample the cold, outer regions of the disk, it may be impossible to separate γ from r_2 without resolved disk images.

ξ — Backman and Paresce (1993) report that ξ ranges from $1/2\pi$ to 2π. The models in this paper use $\xi = 1$, which corresponds to a moderate absorber. This means $\lambda_0 = a$.

M — The disk models in this paper permit masses of any value. Because these models are single grain-size, and exclude the most massive objects of the disks, all of the derived masses are undervalued. One of the important reasons to study circumstellar disks is to determine their mass evolution. Does the disk have enough mass to form planets? Have planets already formed? To get a more accurate mass estimation, the disk models will need to have a distribution of grain sizes, and will have to accurately adopt grain density, and grain efficiency constants.

3.5. Best-Fit Results

The first way to evaluate the effectiveness of this modeling system is to construct best-fit models, and grade them with the χ^2_ν statistic. I use the Levenberg-Marquardt algorithm to follow the $\chi 2$ statistic "downhill" in parameter space to a local minimum. The χ^2_ν statistic is calculated by dividing $\chi 2$ by the degree of freedom (# of data points minus # of fit parameters). Because the stars in the FEPS survey usually have significant infrared excesses in only two or three data points,

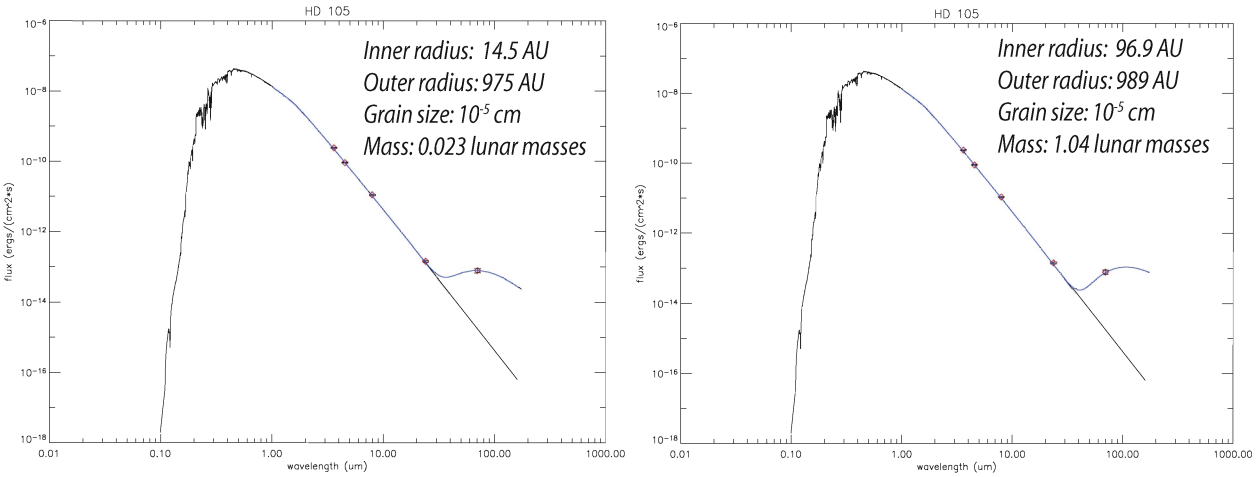

Fig. 4.— Best-fit disk models are useful for checking to see how well specific kinds of models fit. But with few data points and many modeling parameters, drastically different disk models can fit the same data equally well.

the number of parameters I can fit is severely limited. I calculate the best-fit model using assumed values for all parameters except r_1, r_2, and σ or M. The assumed grain size, a, has the biggest effect on the model's outcome, while γ has a negligible effect, and p and q have large effects for some stars but not all. Ultimately the Levenberg-Marquardt algorithm fails because of the complicated structure of $\chi 2$ in parameter space, which is riddled with local minima, and because there is not enough data to fit all parameters while maintaining degrees of freedom (see Fig. 4).

The Levenberg-Marquardt best-fit results are useful for testing models with specific properties (like $a = 10^{-4}\ cm$ for example), but do not do a good job of sampling the best-fit results from all space. To do that, I construct a grid of up to $5 \cdot 10^7$ models for each star (used in the marginal probabilities section below), and treat the model with the lowest $\chi 2$ as an estimate for the global best-fit model. I then use the Levenberg-Marquardt algorithm to zoom in to the best-fit result at the local minimum of my guess. Even using this technique, there are many models that fit almost as well as the "global best-fit", but I choose a single model as representative. Results are presented for HD 105 and HD107146 (see Figs. 5-6 and Table 2).

In the rest of this paper, I abandon the best-fit technique and use the methods of Bayesian statistics and marginal probabilities to combine the results of many models. By doing this, I can calculate the probabilities of specific disk parameters, but I lose the ability to describe the system with individual, complete models.

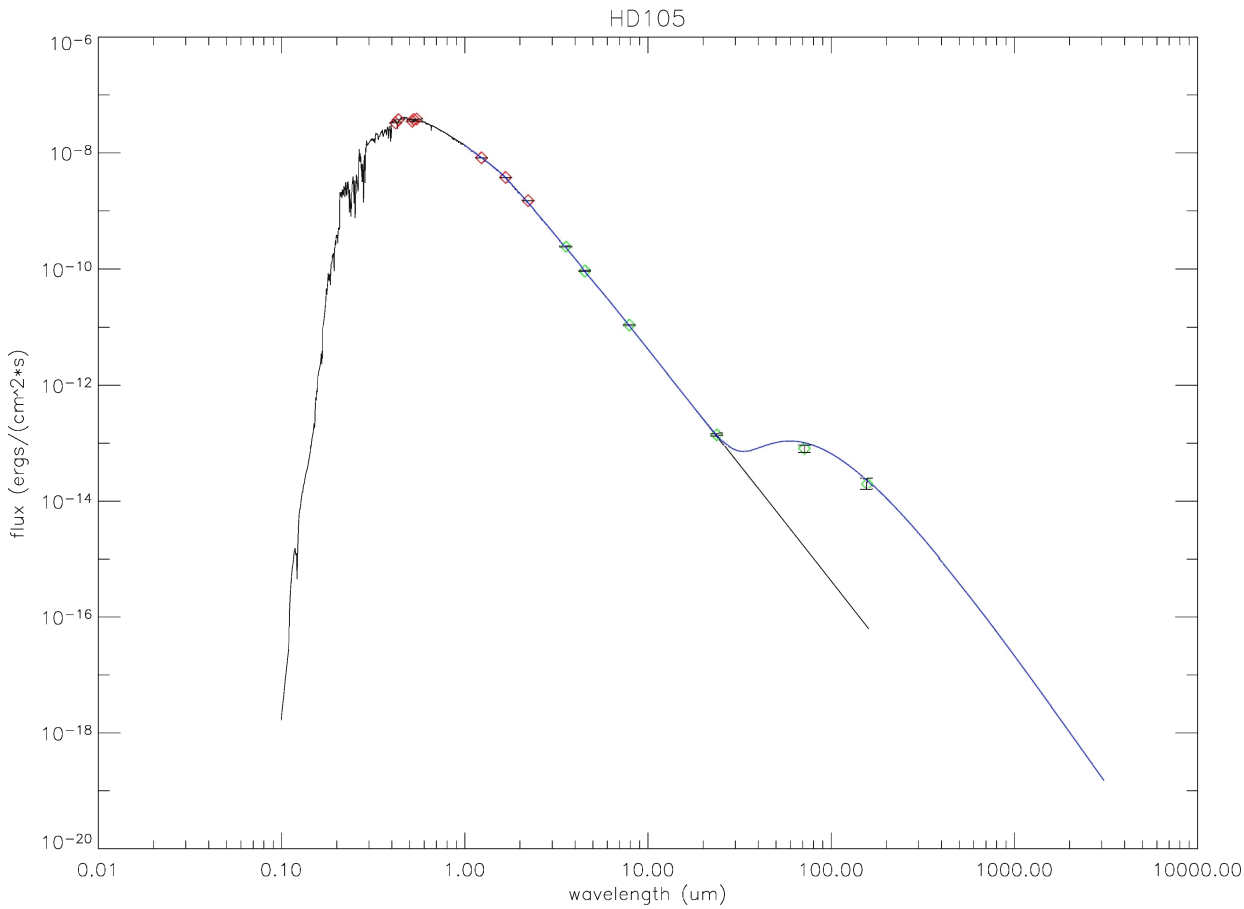

Fig. 5.— **Best-Fit Model Results for HD 105**–The red diamonds are optical and near infrared photometry points fit to a model atmosphere (black curve). The green diamonds are compared with the model atmosphere, and their excesses are fit to a circumstellar disk model (blue curve). This particular model fit is the global best-fit model for HD 105 in the parameter space defined in the marginals section. I first estimated the global best-fit by taking the lowest $\chi 2$ model out of a 1,920,000 model grid. Then I used the Levenberg-Marquardt algorithm to improve the estimate. The results of this model are summarized in Table 2.

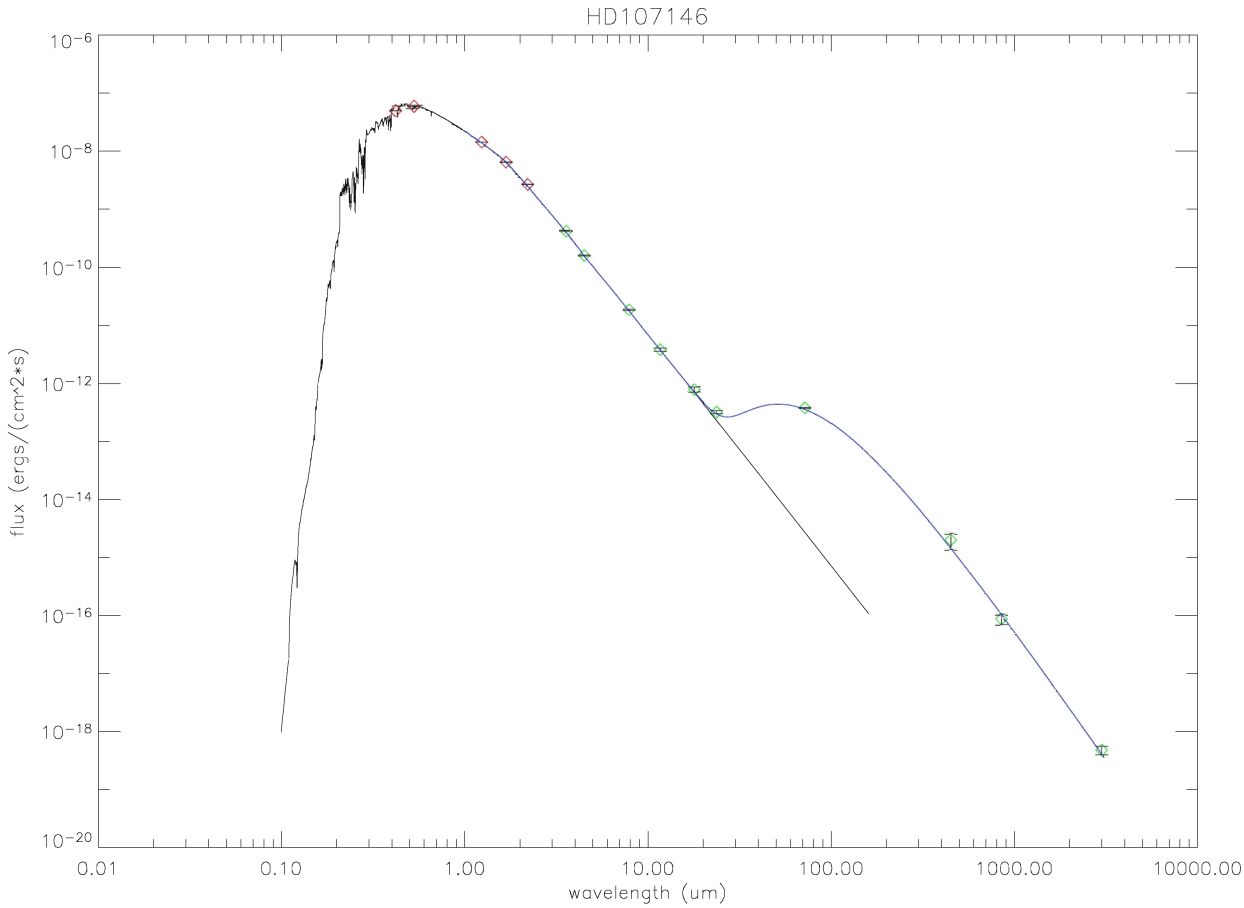

Fig. 6.— **Best-Fit Model Results for HD 107146**–The same methods described in Fig. 5 are employed here. In the case of HD 107146, I use a grid of 3,840,000 models.

	HD 105	HD 107146
r_1(AU)	70.7	33.1
r_2(AU)	470.3	248.4
$\sigma_0(cm^2/cm^2)$	4.89	0.36
$M(M_{lunar})$	0.182	1.244
a (cm)	1.87e-5	8.44e-4
p	1.5	0.0
q	0.5	0.5

Table 2: Output of the models shown in Figs. 5 and 6. In the case of HD 105, I have modeled an optically thick disk (see σ_0), which is therefore physically inaccurate.

4. Marginal Probabilities

4.1. Construction of a Bayesian Grid of Relative Probabilities

Unlike common frequentist statistics, which are used to calculate the probability that data could have come from a model, Bayesian statistics can be used to calculate the *plausibility* of a model, based on data. For many experimental and observing applications, the plausibility of a model is the more useful piece of information. Since the models in this paper depend on many quantities, it is useful to form a grid of models and construct a probability distribution in parameter space. I use Bayesian statistics to calculate the relative probability of each model on the grid.

Bayes' theorem states

$$P(X \mid Y, I) = \frac{P(Y \mid X, I) \cdot P(X \mid I)}{P(Y \mid I)} \tag{4}$$

where I is background information, and X and Y are correlated random variables.

Relating this to a model and data gives

$$P(model \mid data, I) = \frac{P(data \mid model, I) \cdot P(model \mid I)}{P(data \mid I)} \tag{5}$$

Let's evaluate the right side of the equation term-by-term (derivation follows Sivia (1996)):

4.1.1. $P(data \mid I)$

The background information I have is mostly literature based (for example, Jewitt and Luu (2000) give the outer radius of Beta Pic to be about 1000 AU, so I know that 1000 AU is a reasonable outer limit of a circumstellar disk). The observed data is certainly correlated to the background information, but it is impossible to tell how, so $P(data \mid I)$ is unknown. However, for a given set of data (1 star), $P(data \mid I)$ is constant for every model, so we can drop it into a proportionality.

$$P(model \mid data, I) \propto P(data \mid model) \cdot P(model \mid I) \tag{6}$$

We will normalize later to remove the proportionality.

4.1.2. $P(data \mid model)$

Let $data$ comprise n data points: $data_1$, $data_2$, ... , $data_n$.

$$P(data \mid model) = P(data_1 \mid model) \cdot P(data_2 \mid model) \cdot \ldots \tag{7}$$

$$= \prod_{i=1}^{n} P(data_i \mid model) \tag{8}$$

Now if we assume that the measurement errors are normally distributed so that $data_i$ can be written as a Gaussian with $\mu = model\,value_i$ and $\sigma = \sigma_{data_i}$, then

$$P(data_i \mid model) = \frac{1}{\sqrt{2\pi}\sigma_i} e^{\frac{-(model\,value_i - data_i)^2}{2\sigma_i^2}} \tag{9}$$

$$P(data \mid model) = (\frac{1}{\sqrt{2\pi}})^n \cdot \prod_{i=1}^{n} \frac{1}{\sigma_i} \cdot e^{-\frac{\chi^2}{2}} \tag{10}$$

We can drop $(\frac{1}{\sqrt{2\pi}})^n \cdot \prod_{i=1}^{n} \frac{1}{\sigma_i}$into the proportionality because, as long as we use the same data, it will be the same for every model. Then

$$P(data \mid model) \propto e^{-\frac{\chi^2}{2}} \tag{11}$$

4.1.3. $P(model \mid I)$

For $P(model \mid I)$, the prior distribution, we set upper and lower bounds on each of our model parameters which gives $P(model \mid I) = 0$ for all models outside of our grid. Since we do not know much else from background information, our best guess should be to assume uniform probability over all grid models. Then $P(model \mid I)$ will drop out of the proportionality. However, the physical parameters (r_1, r_2, $mass$, and a) would be more appropriately distributed as uniform in log-space (Harvey and Jefferys 2000). If we want $P(model \mid I)$ to drop out of the equation, we will need to institute our priors through grid spacing—so the model grain sizes and etc. will be distributed uniformly in log space.

The final relative probabilities for each model are given by

$$P(model \mid data) \propto e^{-\frac{\chi^2}{2}} \tag{12}$$

which can be normalized to construct an n-parameter probability distribution, $P(x_1, \ldots, x_n)$.

4.2. Method of Marginal Probabilities

By the method of marginal probabilities, we can restore an independent probability distribution function for each free parameter by integrating over the other free parameters (see Fig. 7).

$$P(x_1) = \int_{-\infty}^{\infty} \ldots \int_{-\infty}^{\infty} P(x_1, \ldots, x_n) dx_2 \ldots dx_n \tag{13}$$

In practice, I do not integrate from $-\infty$ to ∞. I set upper and lower bounds on the parameters based on the literature and previous trials (this is part of the Bayesian prior). The multi-variable integration and grid-model calculation can be extremely computationally intensive which sets a limit on the precision of my trapezoidal integration.

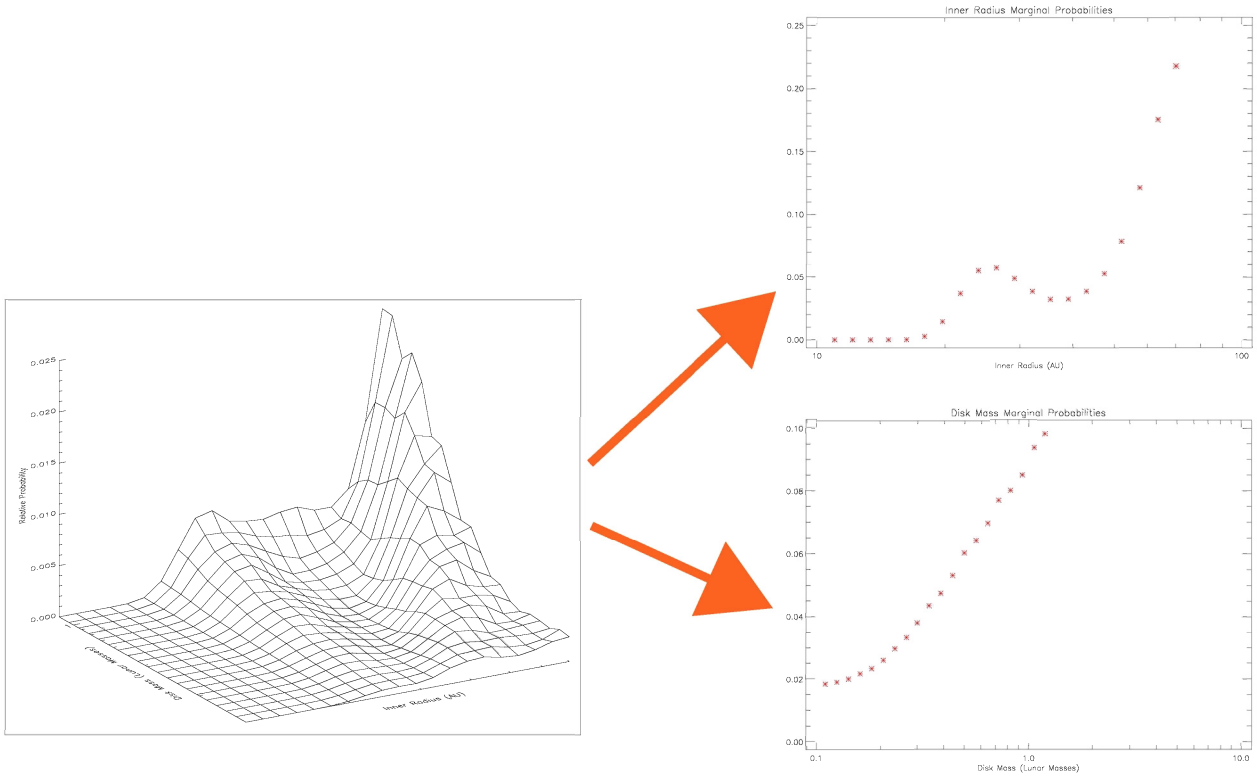

Fig. 7.— The 2-D probability distribution is separated into independent 1-D plots using the method of marginal probabilities. In this paper, I use the technique to transform a 7-D model grid into seven individual probability distributions for important disk parameters.

5. Results of Bayesian/Marginal Model Fitting

The Bayesian/marginal statistics analysis method is useful for consolidating information from many models. For a problem with lots of data and a simple model, it may be possible to fit a single best-fit model to the data, but when multiple models can fit the data without drastically different $\chi 2$ statistics, the method of Bayesian/marginal statistics should be used to construct distributions of individual parameters. The usefulness of this technique stems from the fact that it gives fair weighting to well-fit models and badly-fit models; the relative probability of many mediocre models may surpass the relative probability of a single good model.

In the context of this project, I am interested in fitting seven disk parameters and evaluating their marginal probabilities. The ultimate goal of the project is to constrain the disk parameters by constructing marginal distributions with limits. I have chosen three example stars for this paper:

HD 105 is a FEPS star with good optical data (for the photosphere fit) and exceptional Spitzer data. It was one of the only FEPS stars with IRAC 5.8 μm data (though for HD 105, the 5.8 μm data does not fit well with the other IRAC data), and it was a star with definite excess in the MIPS 70 and 160 μm bands, with small errors on each of those respective points. The results for HD 105 demonstrates Spitzer's sensitivity to the disk parameters, independent of ancillary data.

HD 107146 is a nearby FEPS star with great millimeter ancillary data and a resolved circumstellar disk in scattered, optical light from the Hubble Space Telescope. KECK, SCUBA, and SEST data are all available for HD 107146 (see Appendix B), and all have small enough errors to help constrain disk parameters. Bayesian/marginal statistics results are compared to the resolved Hubble image, and the usefulness of long-wavelength data is discussed.

HD 115043 is a FEPS star that shows no infrared excess in MIPS 24 or 70 μm data (it has no MIPS 160 μm data). The point of fitting this star with circumstellar disk models is to demonstrate the results of a Bayesian/Marginal statistics non-detection. A non-detection using these methods can be defined as a set of results that cannot put a lower limit on mass.

For each of these stars, I calculate the marginal distributions for r_1, r_2, $mass$, γ (except for HD 107146), a, p, and q. For the two stars with disks, HD 105 and HD 107146, r_1 and $mass$ can be constrained to unimodal, Gauss-like distributions. p is constrained for both stars, and q is constrained for HD 107146. a is not constrained within the narrow band of my models that are considered accurate (see section 3.4). r_2 is not constrained for either star. γ has a uniform, marginal probability over the range described in section 3.4. It is completely unconstrained by the data using this method.

5.1. The Bayesian Prior

The Bayesian Prior for the methods described in this paper is applied through grid spacing as described in section 4.1.3. I assume that the a priori probabilities of the parameters (r_1, r_2, $mass$, and a) are distributed uniformly in log space. The power-law exponent parameters (γ, p, and q) are assumed to be distributed uniformly. The range of the grid spacing is determined partially by prior, literature-based limits as described in section 3.4, and partially by adjusting the ranges of previous trials so as to construct marginal distributions with limits. For example, if a run shows that the largest value considered has a non-zero probability, I repeat the run with a higher prior constraint. The resolution of the grid is also adjusted based on the results of previous trials to provide the desired modeling power where needed. Certain models are removed from the grid for physical reasons: I do not evaluate models that have $r_2 < r_1$ because the disk cannot have negative mass, and I do not evaluate disks with $p < q$ because this would be an unphysical grain emission/absorption model. This affects the uniformity of the prior distributions in complex ways: because there are fewer possible models with $q = 0$ than $q = 0.5$, I am implicitly assuming that $q = 0$ is less likely than $q = 0.5$. This is a concern that will be addressed in later stages of the project.

5.2. Interpreting the Results

Each set of results includes seven graphs (except for HD 107146, which has six), one for each marginalized parameter. The x-axis of each graph shows the range of the parameter while the y-axis shows the relative probability of each data point. The total probability of the data points for a single graph adds to one. Each point on a single graph has been calculated by integrating over all points in every other plot (see Eq. 13). Therefore, the total number of models calculated is the product of the number of points in each graph. In a couple of graphs, the results are somewhat jagged. Since each point is calculated by integrating the probabilities of the other 6 plots, the jaggedness of a plot usually indicates that one or more of the other parameters needs to have better resolution. The graphs are plotted as discrete points, and that is truly how they should be interpreted; the models are evaluated at discrete points, not over a continuous range.

5.3. Results for HD 105 (As Shown in Figure 8)

The inner radius is well constrained in a unimodal distribution, although for the prior I have chosen, the largest inner radius models never quite get down to zero-probability. Also, there are three large inner radius points that sit above the rest of the curve. These are the result of the low resolution prior used for the outer radius and the condition that $r_1 < r_2$. The two largest inner radii can only be modeled with the largest outer radius point.

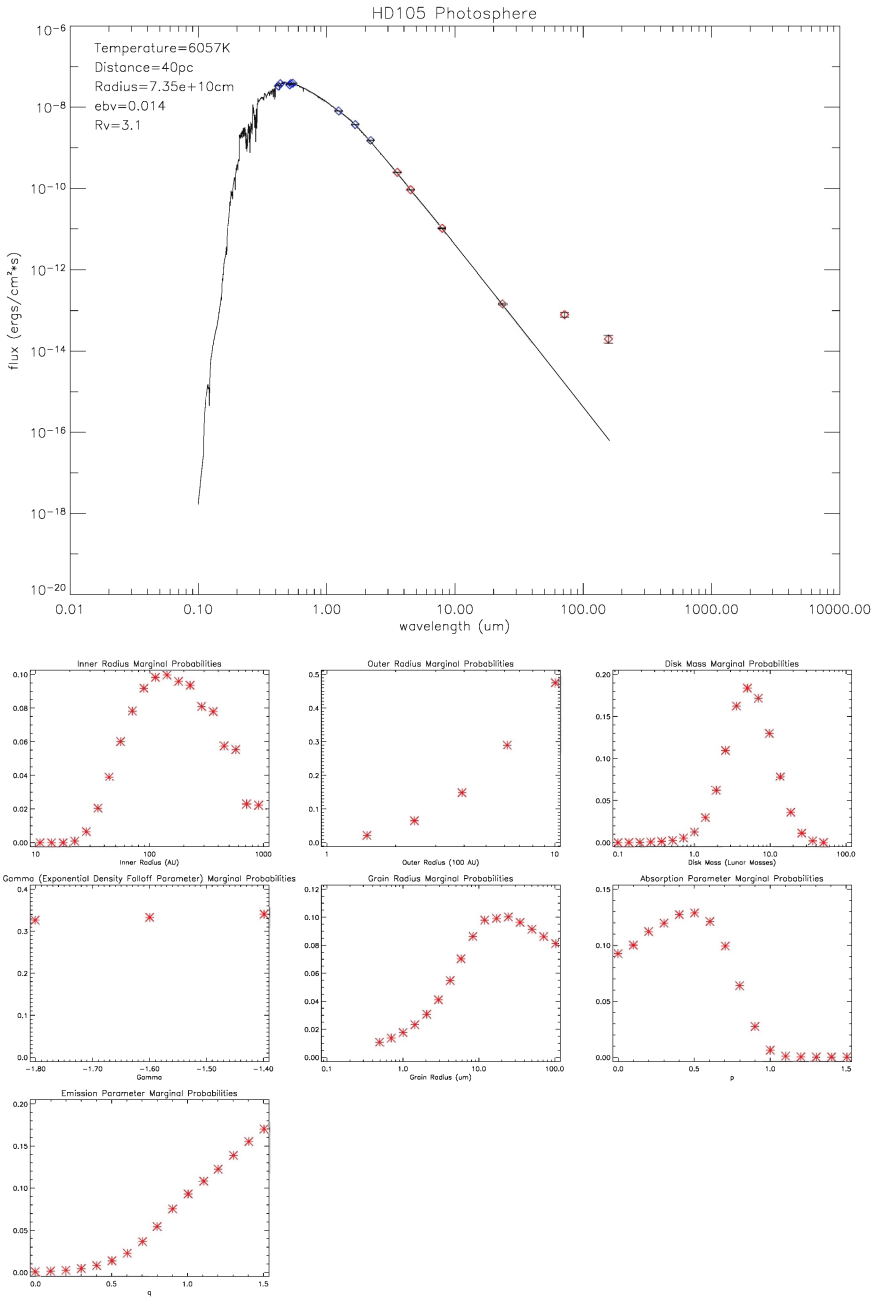

Fig. 8.— **SED and Marginal Distributions for HD105**–The top graphic shows the model atmosphere of HD 105 in black and data points with error bars. The blue data points are used to fit the model atmosphere, and the red points are used to calculate infrared excesses, which are then used to model the circumstellar disk.

The bottom graphic shows the results of the Bayesian/Marginal method for HD 105. The x-axis of each graph shows the range of the parameter while the y-axis shows the relative probabilities for each data point. The total probability of the data points for a single graph adds to one. The prior grid contains ~ 25 million models.

The outer radius is not well constrained, as should be expected because dust from circumstellar disks eventually blends with the interstellar medium, and the coolest dust does not emit much light anyway. Still, for the modeling equations I use, it is necessary to have an outer disk radius, and it may be worth investing some integration time to smooth out the other curves.

The disk mass is very well constrained in a Gaussian-like distribution. With the assumptions I have made ($\rho = 5\ g/cm^3$, spherical, single grain-size model with $a < 100\ \mu m$, etc.), I can list the disk mass as between 1.0 and 20.0 lunar masses with 98% confidence.

The surface density exponent γ is not constrained at all for HD 105, nor is it for any other star using this type of data. This parameter cannot be properly isolated without a statistical sample of resolved disks. Thus, to save modeling time, I fix γ in some models below.

The grain radius distribution has a peak at about 11 μm, but does not converge to 0 inside the boundaries described in section 3.4. Grain radius and mass are highly correlated, so adjusting the disk model to allow larger grains and grain distributions is a high priority for future stages of this project.

p is well constrained on both sides (p cannot be < 0 because that would imply that grains absorb better at long wavelengths than at short wavelengths) while q is only well constrained at its smaller end. However, if the examples of p and q given by Backman and Paresce (1993) are exhaustive, then we do not have to worry about $q > 1.5$. The next step in further constraining p and q is to use a non-uniform prior based on laboratory tests of dust emission and absorption. As will be shown in sections 5.4 and 5.6, mm data can be used to constrain p and q

5.4. Results for HD 107146 (As Shown in Figure 9)

The long-wavelength data for HD 107146 does a much better job of constraining the inner radius than Spitzer data alone could do for HD 105. While the upper limit of inner radius for HD 105 is 1000 AU, it is only 100 for HD 105. The jaggedness in the r_1 distribution is probably an artifact of low resolution in one of the other parameters (probably p and/or r_2).

The outer radius is constrained in a similar way to that of HD 105, except the slope of the curve is less steep. This is probably because there are more possible models evaluated at the large r_2 points than the small ones for HD 105 given the condition $r_1 < r_2$ (see the discussion in section 5.1) .

In this particular run, I have not included a graph of γ's probability distribution. From other trials on HD 105 and HD 107146, I am confident, that the results for other parameters are independent of my choice for γ, so I use $\gamma = -1.6$ for the HD 107146 marginals method. This allows me to spend my modeling power on more important parameters.

p and q are both nicely constrained for HD 107146.

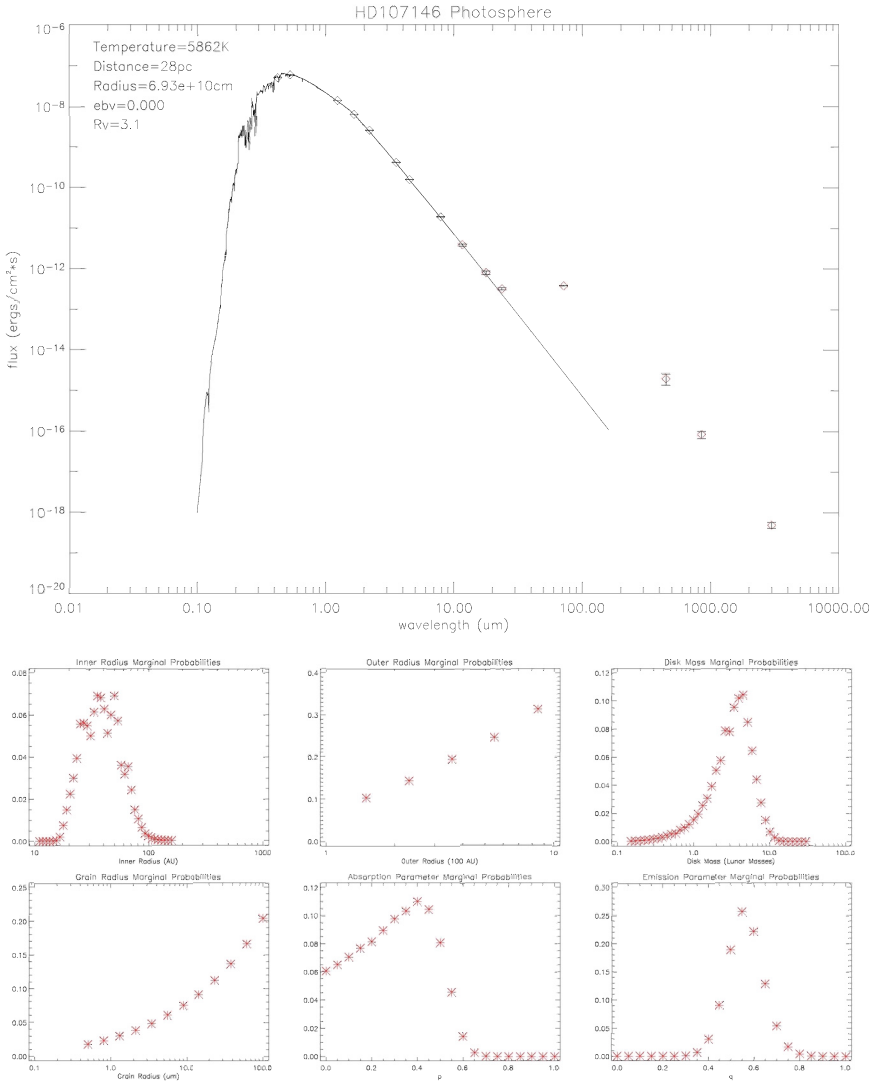

Fig. 9.— **SED and Marginal Distributions for HD107146**– The same methods described in Fig. 8 are employed here. In the case of HD 107146, I use a prior grid containing $\sim$ 46 million models.

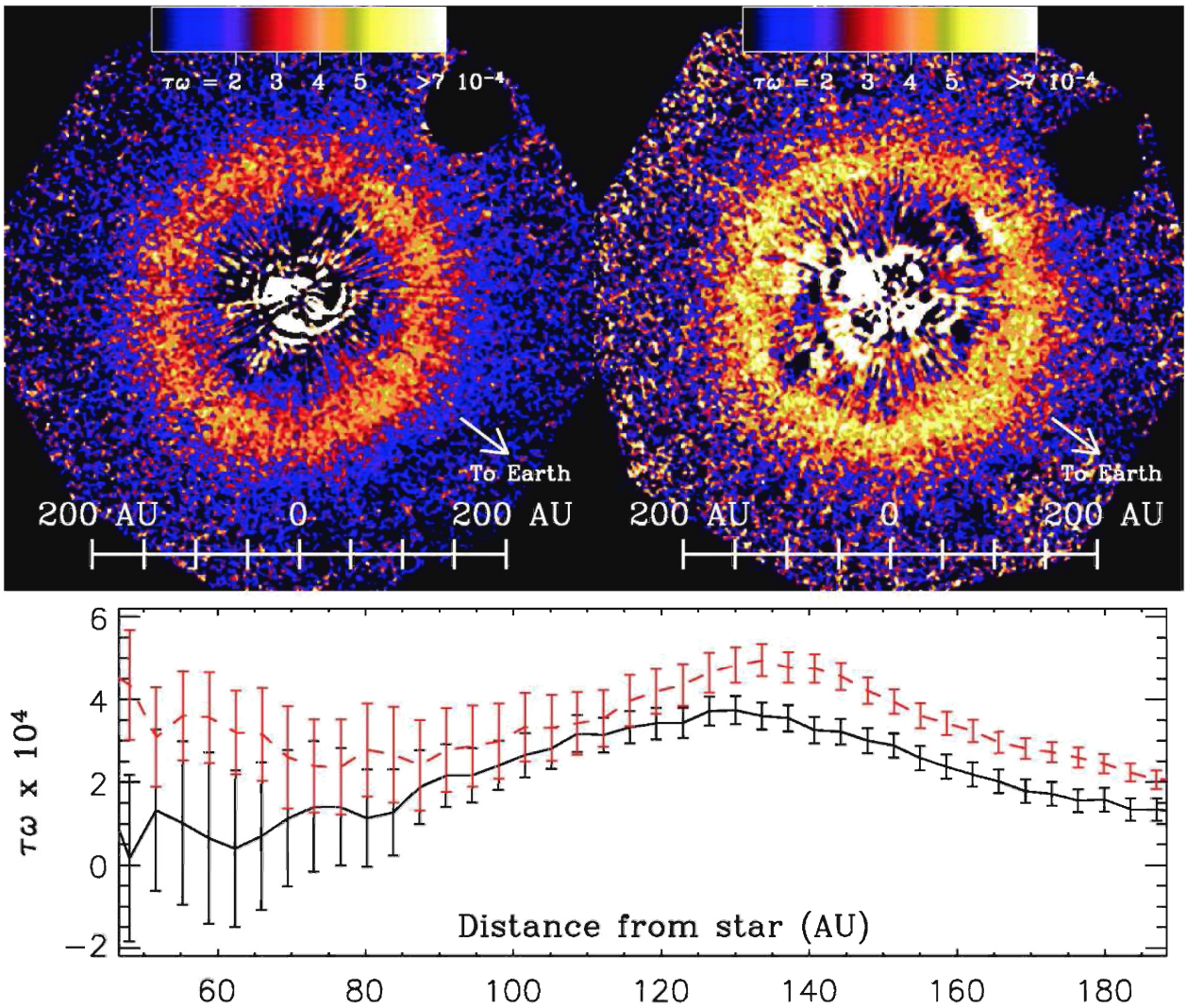

Fig. 10.— Combines Figure 1 and Figure 3 from Ardila *et al.* (2005).
Top: Images of HD 107146 taken in scattered light. The images have been corrected to provide maps of scattering optical depth ($\tau\omega$), which is related to the quantity used in this paper, σ. The top left image is from the Hubble F606W filter (broad V), and the top right image is from the Hubble F814W filter (broad I).
Bottom: Median scattering optical depth of the disk as a function of radius. The black, solid curve is for the F606W filter, and the red, dashed curve is for the F814W filter. The plot clearly show that scattering optical depth peaks near 130 AU and that $r_1 < 80$ AU, which is consistent with the results derived in this paper from Spitzer, Keck, SCUBA, and SEST data.

Ardila *et al.* (2004) have published the results of a resolved debris disk around HD 107146 using scattered light in Hubble's F606W filter (broad V) and F814W filter (broad I). Their results indicate a ring-shaped disk centered at 130 AU with a FWHM of 85 AU. Because of the coronagraph and point-spread subtraction, the authors do not exclude the possibility that dust exits inside a 60 AU ring, but they do show that the disk's surface density decreases inside of 130 AU (Ardila *et al.* 2004). My results for inner radius are consistent with the results of the resolved image, although the resolved disk clearly has a more complex radial density profile than the one I have assumed.

5.5. Results for HD 115043 (As Shown in Figure 11)

The results for HD 115043 are as might be expected for a star with no infrared excess. The large inner radius models are more probable than the small inner radius models; at large radii, the dust is cool and emits less light than warm dust close to the star. Also, as would be expected, relative probabilities are highest for the least massive disks. The individual grains are as large as possible so that the disk can contain some mass without emitting much light.

The Bayesian/marginal statistics method does not answer the most important question for a star with no infrared excess: what is the upper limit on mass for a circumstellar disk around this star? If I allowed my prior for mass to increase its range in the low mass direction, the curve would eventually flatten out (a 1 g circumstellar disk has the same relative likelihood as a 10 g circumstellar disk), but because the data cannot produce a lower limit on mass, it is impossible to normalize the curve, and I cannot assign an absolute probability to the higher mass models. The standard χ^2 fitting techniques might be the best way to approach this problem for a star with no infrared excess.

5.6. Analysis of Results for HD 107146 which Exclude Long-Wavelength Data-(As Shown in Figure 12)

One of the goals of this paper is to establish the level of constraint expected for other FEPS stars based on their available data, and demonstrate a purpose for future long-wavelength observations. I use HD 107146 as an example star, and compare the results of the Bayesian/marginals method on a full data set with the results of a data set that is missing the long wavelength data (SCUBA 450 and 850 μm, and SEST 3.0 mm). Figure 12 shows the marginal probabilities of six disk parameters with the inclusive results plotted in red and the exclusive results plotted in blue. Because the blue curves' data is a subset of the red curves' data, I consider the red curve to be the more accurate representation of the disk's true properties.

The marginal results for r_1 indicate that long-wavelength data helps constrain the upper range for inner radius. The blue curve does not quite converge with 0-probability in the particular prior I have chosen, but after its slope flattens, it looks like it will reach about 300 AU before the relative

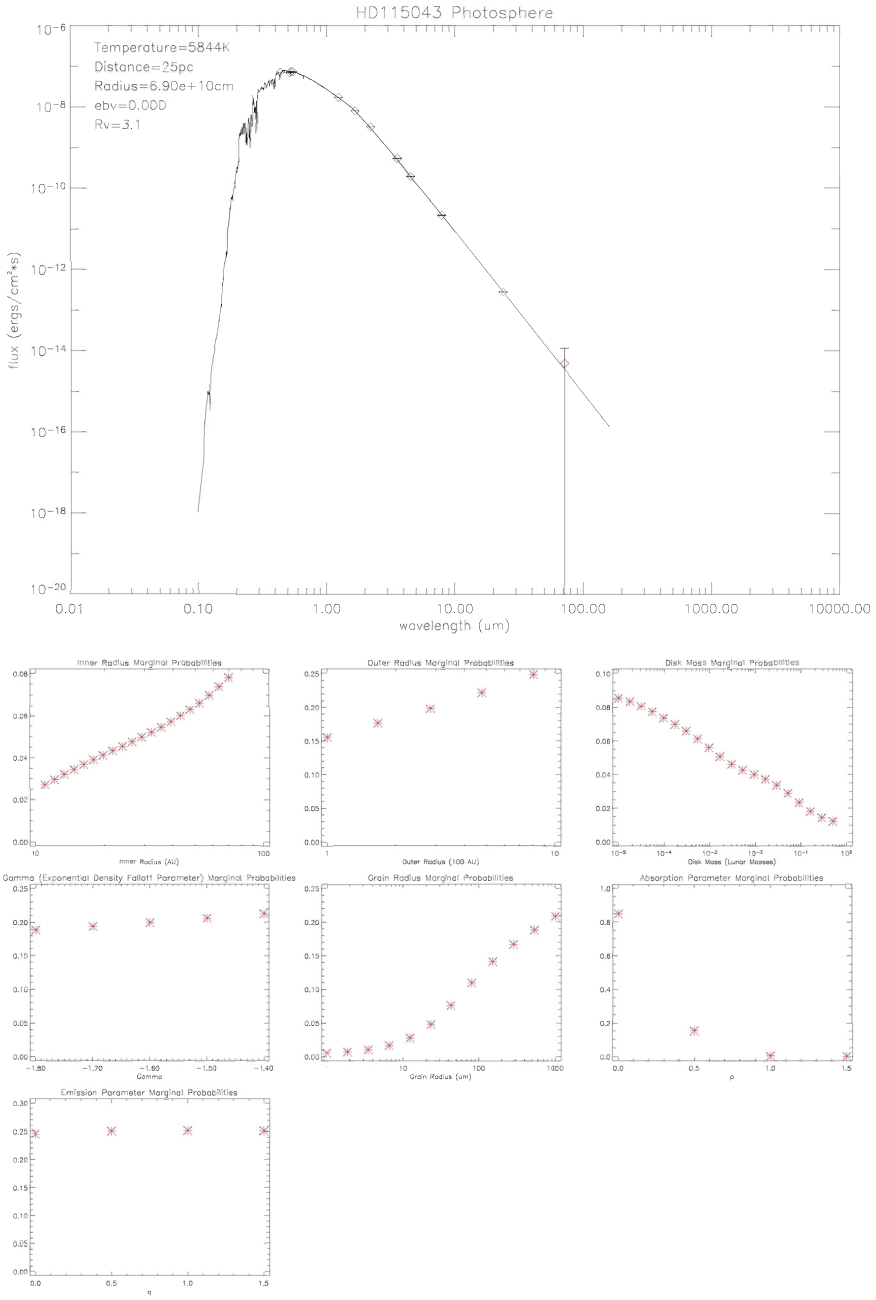

Fig. 11.— **SED and Marginal Distributions for HD115043**– The same methods described in Figs. 8 and 9 are employed here. In the case of HD 115043, I use a prior grid containing $\sim$ 2.5 million models.

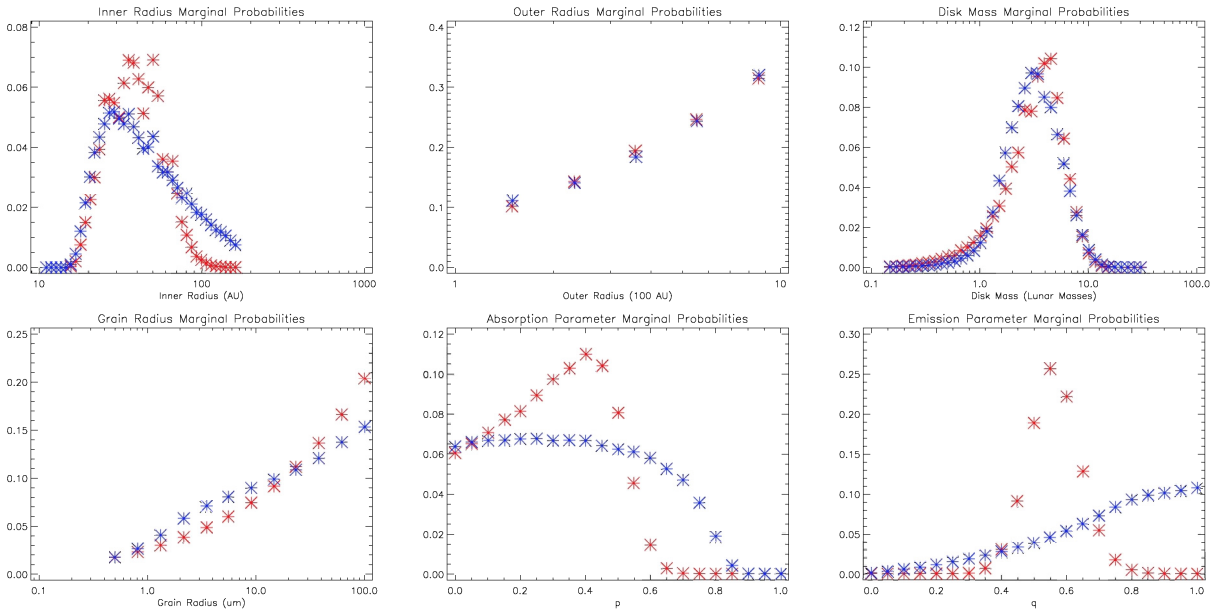

Fig. 12.— Marginal Probabilities of disk parameters for HD 107146. The red points include long-wavelength, ancillary data (SCUBA 450 and 850 μm, and SEST 3.0 mm) while the blue points exclude them. The two sets of data are products of the same prior (also used in figure 9), and both use all available KECK and Spitzer data (see Appendix B).

probabilities become arbitrarily small. Compare this with the red curve which is constrained at about 100 AU.

The marginal results of r_2, $mass$, and a are similar for the two cases.

The most drastic difference between the results of the two data sets is for p and q. q has its biggest effect on long-wavelength emission, which is why the long-wavelength data is so important for constraining it. The change in the shape of the p-curve is most likely a result of the condition I have imposed that $p < q$. A similar set of results to the blue curve is shown in figure 12 for HD 105, which has no mm data.

Long-wavelength data is necessary for constraining p, q, and the outer constraint of r_1. Carpenter *et al.* (2005) SEST measurements are helpful for a lot of the FEPS stars, but more data and/or smaller error bars are necessary for the types of constraints that are the goal of this project and its techniques.

6. Conclusion

6.1. Summary

The structure, evolution, and dust contents of circumstellar disks are important for tracing the formation of planets. Determining the model types and parameter constraints is an interdisciplinary field that includes laboratory physics, theory, direct space measurement, observation, computer modeling, and statistical inference. The Spitzer Space Telescope is a powerful new tool for observing disks in a wavelength range (which includes the disks' peak emission) that was previously impossible. Stars that have infrared excesses in Spitzer wavelengths are likely surrounded by circumstellar disks, and by subtracting out the contribution of the stellar photosphere, I am able to model disks to the infrared excesses. Because single, best-fit models only tell us what types of models fit and whether models fit at all, I use the techniques of Bayesian statistics and marginal probabilities to construct probability distributions for important disk parameters.

HD 105 and HD 107146 have infrared excesses, which I have analyzed with the Bayesian/marginals technique. For HD 105, r_1, $mass$, and p are constrained. For HD 107146, r_1, $mass$, p, and q are constrained. γ and r_2 cannot be constrained. a is not constrained using the models from this paper. It is likely that a multiple grain-size model with accurately represented large-grain emission would constrain large a, and a detailed study of radiative grain removing processes would constrain small a. Until a is constrained, all mass estimates are only accurate in the context of single-grain models where $a < 100\ \mu m$; the physically pertinent question, how much mass is orbiting the star, cannot be answered by the current models.

6.2. Future Steps

6.2.1. Improvement of Models

The results of this paper point to some necessary changes that should be made to the disk models. The most obvious fault of the models is the unphysical emission/absorption approximation described in section 3.3. Removing the approximation will cause the disk modeling equations in section 3.2 to become non-analytic and will add computation time to each model, but doing so will allow large grain models, which are necessary for modeling a disk with a distribution of grain sizes. This is the only way to accurately determine disk mass.

6.2.2. Direct Measurements of Grains

To improve the disk mass estimate, more information is needed about the shape and density of circumstellar dust grains. Spherical grains have the least possible surface-area/luminosity ratio for a given mass, so if real circumstellar disks have irregular grains, the disk's mass will be lower than

the model disks. Grain shape distributions will likely be the result of direct measurement of Solar System dust. Also, this would allow more accurate modeling of dust absorption/emission/scattering properties.

6.2.3. Improvement of Priors

In this paper I have used uniform priors to describe my best initial guess for the probability distributions. In reality, we know that the distributions are not going to be uniform (they will probably be unimodal), and the prior should reflect this knowledge. Constructing a prior would be an enormous undertaking, which would involve using the Bayesian/marginal method on a large sample of circumstellar disks. Presumably, such a prior distribution would be age dependent and could be iterated with a sample of many circumstellar disks.

6.2.4. Construction of Marginal Distributions Whose Endpoints Converge with Zero

Ultimately, the goal of the Bayesian/marginals method is to allow parameter estimation with error analysis and confidence limits. The best scenario would be to fit Gaussian curves to parameter distributions. In most cases, this will be possible with sufficient integration (equation 13).

A. Discussion of Disk Model Equations

A.1. Derivation of the Temperature Equation in Backman and Paresce (1993)

We assume the star and the grains emit thermally, like blackbodies, although not perfectly efficient ones. To find the equilibrium temperature of the grains as a function of radius, we find T_{dust} where the grains emit the same amount of energy that they absorb.

$$g_1 \pi a^2 (\frac{R_{star}}{r})^2 \int_0^\infty \pi \epsilon_\nu B_\nu(T_{star}) d\nu \tag{A1}$$

$$4 g_2 \pi a^2 \int_0^\infty \pi \epsilon_\nu B_\nu(T_{dust}) d\nu \tag{A2}$$

A1 is the energy absorbed by a dust grain and A2 is the energy emitted by a dust grain. g_1 and g_2 are geometric factors related to a dust grain's shape, rotation, and conductivity. Set $g_1 = g_2$ for a dust grain whose entire surface is at an equilibrium temperature, T_g. Now set the absorbed energy equal to the emitted energy to solve for the equilibrium gas temperature.

$$(\frac{R_{star}}{r})^2 \int_0^\infty \epsilon_\nu B_\nu(T_{star}) d\nu = 4 \int_0^\infty \epsilon_\nu B_\nu(T_{dust}) d\nu \tag{A3}$$

Backman and Paresce (1993) suggest using a power law decay for ϵ_ν so that for $\lambda > \lambda_0$, $\epsilon_\nu \sim \epsilon_0(\lambda_0/\lambda)^p$ for absorption (the left side of A3), and $\epsilon_\nu \sim \epsilon_0(\lambda_0/\lambda)^q$ for emission (the right side of A3). In doing the derivation, Backman and Paresce (1993) have left out the condition $\lambda > \lambda_0$ so that emission can be greater than 1 for $\lambda < \lambda_0$, which is unphysical. The equation becomes

$$(\frac{R_{star}}{r})^2 \int_0^\infty \epsilon_0 (\frac{\lambda_0}{\lambda})^p B_\nu(T_{star}) d\nu = 4 \int_0^\infty \epsilon_0 (\frac{\lambda_0}{\lambda})^q B_\nu(T_{dust}) d\nu \tag{A4}$$

The solution to the derivation is as follows:

$$T_{dust} = [\frac{T_{star}^p L_{star}}{16 \pi r^2 \sigma_{SB}} \cdot (\frac{\lambda_0 k}{hc})^{p-q} \cdot \frac{\Gamma(4+p)}{\Gamma(4+q)} \cdot \frac{\Sigma_{i=1}^\infty i^{-(4+p)}}{\Sigma_{i=1}^\infty i^{-(4+q)}}]^{\frac{1}{4+q}} \tag{A5}$$

A.2. Improvement of the Temperature Equation in Backman and Paresce (1993)

If we add in the condition that absorptive/emissive efficiency has a maximum of 1 for $\lambda < \lambda_0$. Now each of the integrals in equation A3 has to be split into two integrals: one from 0 to λ_0, and one from λ_0 to ∞.

$$(\frac{R_{star}}{r})^2 \int_0^{\lambda_0} B_\nu(T_{star})d\lambda + (\frac{R_{star}}{r})^2 \int_{\lambda_0}^{\infty} \epsilon_0(\frac{\lambda_0}{\lambda})^p B_\nu(T_{star})d\lambda$$
$$= 4\int_0^{\lambda_0} B_\nu(T_{dust})d\lambda + 4\int_{\lambda_0}^{\infty} \epsilon_0(\frac{\lambda_0}{\lambda})^q B_\nu(T_{dust})d\lambda \quad \text{(A6)}$$

The solution to the equation is no longer analytic and must be solved numerically.

A.3. Derivation of the Flux Equation

With the help of the temperature equation, we can now solve for the flux received at Earth.

$$F_\nu = \epsilon_\nu B_\nu[T_g(r,a)]\Omega \quad \text{(A7)}$$

$$\Omega = \frac{cross-sectional\ area\ of\ grain}{D^2} \quad \text{(A8)}$$

The disk is optically thin, so we do not have to worry about what angle we see the disk—we see all of it. Since the temperature of the gas is a function of radius, we have to build up the disk out of rings of infinitesimal width. Each ring has circumference $2\pi r$ and width dr. We will add them up by integrating from r_1 to r_2. At each r, the rings have a geometric surface density, σ_0 (in cm^2/cm^2—$area\ of\ coverage/area$). We assume that σ drops off exponentially— $\sigma(r) = \sigma_0 \cdot (\frac{r}{r_0})^\gamma$. If we know the mass of the particles (as a function of radius) then surface density(σ) can be converted to mass density (ρ) where the integral of ρ in 2-D polar coordinates gives mass (see Eq. 3). Thus,

$$F_\nu = \int_{r_1}^{r_2} \sigma_0(\frac{r}{r_0})^\gamma \epsilon_\nu B_\nu[T_{dust}(r,a)]\frac{2\pi r dr}{D^2} \quad \text{(A9)}$$

where B_ν is in cgs so the units on F_ν are $ergs/s \cdot cm^2 \cdot Hz$. For $\lambda < \lambda_0$, $\epsilon = 1$. In most cases, we will be measuring fluxes where $\lambda > \lambda_0$, so $\epsilon_\nu = (\frac{\lambda_0}{\lambda})^q = (\frac{\xi a\nu}{c})^q$. Putting ϵ_ν into A9 gives

$$F_\nu = \int_{r_1}^{r_2} \sigma_0(\frac{r}{r_0})^\gamma (\frac{\xi a\nu}{c})^q B_\nu[T_{dust}(r,a)]\frac{2\pi r dr}{D^2} \quad \text{(A10)}$$

B. Photometry Data

		HD 105		HD 107146		HD 115043	
filter name	wavelength (μm)	flux	error	flux	error	flux	error
B (mag)	0.436	8.12	0.01			7.46	0.03
BT (mag)	0.421	8.226	0.015	7.781	0.016		
V (mag)	0.545	7.52	0.01			6.89	0.03
VT (mag)	0.526	7.577	0.010	7.108	0.010	6.883	0.010
Hp (mag)	0.517	7.6375	0.0010			6.9429	0.0014
J (mag)	1.235	6.464	0.020	5.867	0.023	5.675	0.021
H (mag)	1.662	6.189	0.022	5.611	0.020	5.399	0.021
Ks (mag)	2.159	6.117	0.020	5.540	0.016	5.334	0.017
IRAC1 (mJy)	3.548	1037.1	9.5	1770.9	14.7	2196.0	20.2
IRAC2 (mJy)	4.492	631.4	5.8	1066.7	8.9	1295.9	11.9
IRAC4 (mJy)	7.87	225.2	3.8	393.1	7.1	444.7	7.6
MIPS24 (mJy)	23.68	26.9	1.1	60.2	3.4	51.8	2.1
MIPS70 (mJy)	71.42	135.4	18.0	647.5	13.7	8.2	11.2
MIPS160 (mJy)	155.9	165.8	36.6				
Keck11.7 (mJy)	11.7			175	10		
Keck17.8 (mJy)	17.8			85	8		
SCUBA450 (mJy)	450			130	40		
SCUBA850 (mJy)	850			20	4		
SEST3.0 (mJy)	3000			1.42	0.23		

Table 3: Optical and Spitzer data from FEPS Data Products (Meyer 2005). Keck and SCUBA data from Williams *et al.* (2004). SEST data from Carpenter *et al.* (2005).

REFERENCES

Ardila, D. R., D. A. Golimowski, J. E. Krist, M. Clampin, J. P. Williams, J. P. Blakeslee, H. C. Ford, G. F. Hartig, and G. D. Illingworth, 2004, ApJ **617**, L147.

Ardila, D. R., D. A. Golimowski, J. E. Krist, M. Clampin, J. P. Williams, J. P. Blakeslee, H. C. Ford, G. F. Hartig, and G. D. Illingworth, 2005, ApJ **624**, L141.

Aumann, H. H., C. A. Beichman, F. C. Gillett, T. de Jong, J. R. Houck, F. J. Low, G. Neugebauer, R. G. Walker, and P. R. Wesselius, 1984, ApJ **278**, L23.

Backman, D. E., and F. Paresce, 1993, in *Protostars and Planets III*, edited by E. H. Levy and J. I. Lunine, pp. 1253–1304.

Bessell, M. S., 2000, *Encyclopedia of Astronomy and Astrophysics* (Institute of Physics Publishing, Bristol, UK), chapter Filters.

Burns, J. A., P. L. Lamy, and S. Soter, 1979, Icarus **40**, 1.

Carpenter, J. M., S. Wolf, K. Schreyer, R. Launhardt, and T. Henning, 2005, AJ **129**, 1049.

Carroll, B., and D. Ostlie, 1996, *Introduction to Modern Astrophysics* (Addison-Wesley, Reading, MA).

Cohen, M., S. T. Megeath, P. L. Hammersley, F. Martín-Luis, and J. Stauffer, 2003a, AJ **125**, 2645.

Cohen, M., W. A. Wheaton, and S. T. Megeath, 2003b, AJ **126**, 1090.

Fitzpatrick, E. L., 1999, PASP **111**, 63.

Harvey, P. M., and W. H. Jefferys, 2000, ApJ **538**, 783.

Hines, D. C., D. E. Backman, J. Bouwman, L. A. Hillenbrand, J. M. Carpenter, M. R. Meyer, J. S. Kim, M. D. Silverstone, J. Rodmann, S. Wolf, E. E. Mamajek, T. Y. Brooke, *et al.*, 2006, ApJ **638**, 1070.

Hines, D. e. a., 2005, *FEPS Data Explanatory Supplement*, SSC, Pasadena, CA, version 2.0 edition.

J. Beuzit, e. a., 1997.

Jewitt, D. C., and J. X. Luu, 2000, Protostars and Planets IV , 1201.

Kalas, P., J. Larwood, B. A. Smith, and A. Schultz, 2000, ApJ **530**, L133.

Kurucz, R. L., 1993, VizieR Online Data Catalog **6039**.

Meyer, M. e. a., 2005, Feps third enhanced data release, Spitzer Legacy Product.

Meyer, M. R., L. A. Hillenbrand, D. E. Backman, S. V. W. Beckwith, J. Bouwman, T. Y. Brooke, J. M. Carpenter, M. Cohen, U. Gorti, T. Henning, D. C. Hines, D. Hollenbach, *et al.*, 2004, ApJS **154**, 422.

Sivia, D. S., 1996, *Data Analysis: A Bayesian Tutorial* (Oxford University Press, New York).

Smith, B. A., and R. J. Terrile, 1984, Science **226**, 1421.

Soter, S., J. A. Burns, and P. L. Lamy, 1977, in *IAU Colloq. 39: Comets, Asteroids, Meteorites: Interrelations, Evolution and Origins*, edited by A. H. Delsemme, pp. 121–125.

Williams, J. P., J. Najita, M. C. Liu, S. Bottinelli, J. M. Carpenter, L. A. Hillenbrand, M. R. Meyer, and D. R. Soderblom, 2004, ApJ **604**, 414.

Acknowledgments

First and foremost, I would like to thank my advisor, Eric Jensen, for his invaluable support and stunning patience. I have had the pleasure of learning from him since my first day at Swarthmore College, and his passion for astronomy and teaching are the main reasons I am entering the field today.

I also gratefully acknowledge the support of the National Science Foundation through grant AST-0307830 and the FEPS team, especially John Carpenter for his help with photosphere modeling.